Am J Cancer Res 2026;16(2):520-539
www.ajcr.us /ISSN:2156-6976/ajcr0169977

Original Article

Phellinus linteus polysaccharides inhibit castration-resistant prostate cancer progression possibly via dual modulation of PIK3R1 and PGC-1α: a preclinical evaluation

Wei Wei[1*], Jingyi Huang[2*], Le Xie[3], Zhanping Xu[1], Canbin Lin[4], Ming Chen[4]

[1]Department of Urology, Foshan Hospital of Traditional Chinese Medicine Affiliated to Guangzhou University of Chinese Medicine, Foshan 528000, Guangdong, China; [2]Key Laboratory of Glucolipid Metabolic Disorder, Ministry of Education of China, Guangdong Pharmaceutical University, Guangzhou 510006, Guangdong, China; [3]Department of Pathology, Foshan Hospital of Traditional Chinese Medicine Affiliated to Guangzhou University of Chinese Medicine, Foshan 528000, Guangdong, China; [4]Department of Urology, The First Affiliated Hospital of Guangzhou University of Chinese Medicine, Guangzhou 510405, Guangdong, China. [*]Equal contributors and co-first authors.

Received November 12, 2025; Accepted February 11, 2026; Epub February 15, 2026; Published February 28, 2026

Abstract: Castration-resistant prostate cancer (CRPC) remains a major challenge due to limited treatment options and frequent therapeutic resistance. This study demonstrates that *Phellinus linteus* polysaccharides (PLP), both in the form of drug-loaded serum and as a purified extract, exhibit potent anti-CRPC activity through a dual-axis molecular mechanism. In a castrated PC-3 xenograft model, PLP (400 mg/kg/day) suppressed tumor volume growth by 91.7% and tumor weight growth by 78.0% compared with the control group, showing efficacy comparable to abiraterone/prednisone without hepatorenal toxicity. In vitro, both 30% PLP-containing serum and purified PLP inhibited proliferation, migration, and invasion, and promoted apoptosis while reducing intracellular reactive oxygen species levels in PC-3 and 22RV1 cells. Integrative transcriptomic and multi-omics analyses revealed coordinated downregulation of phosphatidylinositol 3-kinase-protein kinase B-mechanistic target of rapamycin signaling and upregulation of peroxisome proliferator-activated receptor gamma coactivator 1-alpha (PGC-1α). Functional validation showed that overexpression of phosphoinositide-3-kinase regulatory subunit 1 rescued PLP-induced tumor suppression, whereas knockdown of PGC-1α abolished its antioxidative and antiproliferative effects, indicating that both pathways are critically involved. These findings suggest that PLP combats CRPC by simultaneously inhibiting oncogenic signaling and mitigating oxidative stress, positioning it as a promising natural therapeutic candidate for CRPC.

Keywords: Castration-resistant prostate cancer, *Phellinus linteus* polysaccharides, PIK3R1, PGC-1α

Introduction

Prostate cancer is the second most common cancer and the fifth leading cause of cancer-related death in men worldwide, with around 1.5 million newly diagnosed cases per year [1]. The proliferation of prostate cancer cells mainly depends on androgen-related signaling. Following initial treatment, the disease typically progresses to castration-resistant prostate cancer (CRPC) after an average course of 2-3 years, at which point hormonal therapies ultimately lose efficacy [2]. Although patients with CRPC may benefit from palliative surgery or radiotherapy, pharmacotherapy is still important, and novel hormonal agents are now by far the main first-line treatment [3]. Despite these therapeutic advances, the median overall survival for patients with CRPC in clinical trials is about 3 years [4, 5]. In real-world settings, however, the average overall survival is less than 2 years, indicating a still unfavorable prognosis [6]. Recently, there has been growing interest in natural products for cancer therapy. Many herbal compounds exhibit higher synergistic effects, lower toxicity, and potential clinical util-

https://doi.org/10.62347/MJNQ6221

ity in improving quality of life, alleviating symptoms, and potentially enhancing survival outcomes.

Phellinus linteus (Sanghuang) is an important medicinal fungus in traditional Chinese medicine. It is commonly included in effective prescriptions used to treat lower urinary tract symptoms and tumor metastasis. For instance, "Sanghuang Decoction" from *Shengji Zongzhu* incorporates *Quercus* bark (Oak bark) to treat dysuria and hematuria, while "Sanghuang Pill" from *Taiping Shenghui Fang*-composed mainly of *P. linteus*, *Sanguisorba officinalis* (Diyu), and *Coptis chinensis* (Huanglian)-is indicated for tumor-related bleeding, abdominal pain, and other symptoms. Modern research has identified *P. linteus* polysaccharides (PLPs) as the main active components, which are heteropolysaccharides exhibiting a range of biological effects including anti-aging, antioxidant, anti-inflammatory, hepatoprotective, and hypoglycemic activities [7]. Evidence suggests that PLPs possess broad anticancer properties, potentially mediated through immunomodulatory mechanisms that activate host defenses such as lymphocytes and macrophages [8]. Experimental studies have shown that PLPs may directly inhibit tumor cell proliferation by inducing programmed necrosis and cell cycle arrest [9, 10]. However, the therapeutic efficacy and molecular mechanisms of PLP in CRPC have not been explored. This study aims to preliminarily elucidate the in vivo mechanism of action of PLP through experiments, providing a foundation for new drug development.

Materials and methods

Drugs and reagents

PLP with a purity of ≥90% (determined by ultraviolet spectroscopy, batch No. PST240523-09) was purchased from Chengdu PUSH Bio-Technology Co., Ltd. (China). Abiraterone was obtained from CHIA TAI Tianqing Pharmaceutical Group Co., Ltd. (China), and prednisone was sourced from Guangzhou Kanghe Pharmaceutical Co., Ltd. (China).

Cell culture

CRPC cell lines PC-3 (catalog no. IM-H075) and 22RV1 (catalog no. IM-H261) were acquired from Xiamen Immocell Biotechnology Co., Ltd. (China). Cells were cultured in RPMI-1640 complete medium containing 10% fetal bovine serum at 37°C in a humidified atmosphere of 5% CO_2.

Preparation and characterization of PLP

PLP was extracted and purified following a modified version of a previously described method. Briefly, dried *P. linteus* fruiting bodies were decocted in water (1:20, w/v) at 100°C for 3 h, and this process was repeated twice. The combined aqueous extracts were concentrated, deproteinized using the Sevag method, and precipitated overnight at 4°C by adding four 4 volumes of ethanol (final concentration 80%, v/v). The crude polysaccharide was redissolved and further purified by sequential chromatography on diethylaminoethyl-52 cellulose and Sephadex G-100. The main fraction (PLP) was collected, dialyzed, lyophilized, and stored at -20°C. Purity was assessed by high-performance gel permeation chromatography, which showed a single symmetric peak. Monosaccharide composition was analyzed by gas chromatography-mass spectrometry after acid hydrolysis and derivatization. Endotoxin levels were measured using a limulus amebocyte lysate assay and were confirmed to be below 0.1 EU/mg.

Experimental animals

Specific pathogen-free-grade adult female Sprague-Dawley rats and 6-8-week-old male BALB/c nude mice were procured from Guangdong Laidi Biomedical Research Institute Co., Ltd. (China). All animal experiments were approved by the Institutional Animal Care and Use Committee of the Research Center (Approval No. LDSW-SOR-AAP-50-023[02]) and the Medical Ethics Committee of Foshan Hospital of Traditional Chinese Medicine Affiliated to Guangzhou University of Chinese Medicine (Approval No. KY[2024]321-1). All procedures were conducted in strict accordance with the Animal Research: Reporting of In Vivo Experiments guidelines. Animals were housed in standard barrier facilities and humanely euthanized upon completion of the experiments.

Preparation of PLP-containing serum

As PLP may exert its biological effects through interactions with serum proteins or host-derived metabolites following oral administration, drug-containing serum was employed in

subsequent in vitro experiments to better simulate its in vivo pharmacological activity, while the in vivo mechanism remained the primary focus of this study. Eight female Sprague-Dawley rats were randomly divided into two groups: a control group receiving distilled water and a PLP-treated group administered PLP solution at 500 mg/kg via oral gavage (2 mL per dose, twice daily) for seven consecutive days. One hour after the final administration, rats were anesthetized by inhalation of isoflurane (4% for induction, 2% for maintenance) in oxygen at a flow rate of 1 L/min, followed by whole blood collection from the abdominal aorta. The animals were then euthanized under anesthesia via exsanguination. Serum was isolated by centrifugation, filtered through a 0.22 μm membrane, aliquoted, and stored at -20°C.

Cellular phenotype analysis

Cell Counting Kit-8 (CCK-8) assay: PLP-containing serum was serially diluted with RPMI-1640 medium to final concentrations of 0%, 5%, 10%, 15%, 25%, 30%, 40%, and 50%. PC-3 and 22RV1 cells were harvested by centrifugation and seeded into 96-well plates. After 24 hours of incubation with the corresponding serum-containing medium, 10 μL of CCK-8 solution (0.5 mg/mL; Bioss, China) diluted in phosphate-buffered saline (Beyotime, China) was added to each well, followed by incubation for 4 hours. Absorbance was measured at 450 nm using a microplate reader (Thermo Fisher Scientific, USA).

Sulforhodamine B (SRB) assay: Cells treated with PLP-containing or blank serum were fixed with 20% trichloroacetic acid at 4°C for 4 hours. After washing, cells were stained with 0.4% SRB (Sigma-Aldrich, USA) in 1% acetic acid, rinsed again, and air-dried. Bound dye was subsequently solubilized with 10 mM Tris-base solution, and absorbance was measured at 515 nm using a microplate reader.

Wound healing assay: PC-3 and 22RV1 cells were seeded at a density of 2.0×10^5 cells per well and grown to 80-90% confluency. A linear scratch was then created using 10 μL pipette tip. Cell migration was monitored at 0 and 24 hours post-scratch. The wound healing rate was quantified by counting the number of cells that had migrated across the scratch boundary.

Transwell invasion assay: Matrigel-coated Transwell inserts (Corning, China) were incubated for 12 h. Cells (1×10^5 cells/well) were seeded into the upper chamber at a density of 1×10^5 cells per well in serum-free medium, while the lower chamber was filled with medium containing 10% fetal bovine serum as a chemoattractant. After 24 hours of incubation, cells were fixed with formaldehyde, stained with Giemsa solution, and counted under a microscope to quantify invasion.

Apoptosis assay (Annexin V-fluorescein isothiocyanate/propidium iodide [V/PI] Staining): After 24 hours of drug treatment, cells were stained with Annexin V-fluorescein isothiocyanate and propidium iodide (PI) (Beyotime, China) for 15 min in the dark. Flow cytometry (BD Biosciences, USA) distinguished viable (Annexin V^-/PI^-), early apoptotic (Annexin V^+/PI^-), and late apoptotic/necrotic (Annexin V^+/PI^+) cell populations.

Reactive Oxygen Species (ROS) detection: After 24 h of treatment, cells were incubated with 10 μM 2',7'-dichlorodihydrofluorescein diacetate (final concentration 10 μmol/L; Meilunbio, China) for 30 min at 37°C. Fluorescence intensity (Ex/Em = 488/525 nm) was measured by flow cytometry.

Xenograft tumor experiment

Following confirmation of in vitro efficacy, in vivo experiments were conducted. A total of 25 specific pathogen-free-grade male BALB/c nude mice (6-8 weeks old) were anesthetized and underwent bilateral orchiectomy. Human CRPC PC-3 cells were harvested, prepared as a single-cell suspension, and adjusted to a density of 1×10^7 cells/mL in serum-free medium. Following surgical recovery, mice were anesthetized with 0.5% lidocaine via subcutaneous injection, and 100 μL of the cell suspension was injected subcutaneously into the right axilla. When tumor volume reached approximately 100 mm^3, mice were randomly assigned to five groups (n=5 per group) according to a computer-generated randomization list: ① Tumor control (T): 2 mL purified water; ② High-dose PLP (H+T): 400 mg/kg PLP; ③ Medium-dose PLP (M+T): 200 mg/kg PLP; ④ Low-dose PLP (L+T): 100 mg/kg PLP; ⑤ Positive control (A+P+T): abiraterone (130 mg/kg) + prednisone (1.3 mg/kg) (human-equivalent doses).

Table 1. Primer sequences for quantitative real-time PCR

Gene	Primer Direction	Sequence (5' → 3')
GAPDH	Forward	AATGGGCAGCCGTTAGGAAA
	Reverse	GCGCCCAATACGACCAAATC
PIK3R1	Forward	AAGTGCCAGAGTGAAGTGGC
	Reverse	GTCCCGTCTGCTGTATCTCG
Akt	Forward	GGCGGCAGGACCGAG
	Reverse	CGCCTGCTCCCGTCTTC
mTOR	Forward	GCCGCGCGAATATTAAAGGA
	Reverse	CTGGTTTCCTCATTCCGGCT
PGC-1α	Forward	TGAAGGGTACTTTTCTGCCCC
	Reverse	GCACAAACTGGATTCGCCAG

GAPDH, glyceraldehyde-3-phosphate dehydrogenase; PIK3R1, phosphoinositide-3-kinase regulatory subunit 1; Akt, protein kinase B; mTOR, mechanistic target of rapamycin; PGC-1α, peroxisome proliferator-activated receptor gamma coactivator 1-alpha; PCR, polymerase chain reaction.

Treatments were administered daily by oral gavage for 28 days in a volume of 2 mL based on body weight. To maintain blinding during tumor measurement, an independent researcher not involved in treatment administration performed all tumor size measurements at the study endpoint.

Tumor monitoring and liver/kidney function assessment

Nude mice were anesthetized with 2% isoflurane at a flow rate of 1 L/min. Tumors were excised and whole blood was collected from the mice, followed by euthanasia via anesthetic overdose. Tumor volume and weight were recorded. Blood samples were analyzed for creatinine, urea nitrogen, alanine aminotransferase, and aspartate aminotransferase using a biochemical analyzer. Tumor tissues were paraffin-embedded, sectioned, and stained with hematoxylin and eosin for histopathological evaluation.

Transcriptome sequencing (RNA-seq)

Total RNA was extracted from tumor tissues and submitted for RNA sequencing. Sequencing was performed on an Illumina NovaSeq 6000 platform with a paired-end 150 bp strategy. Raw reads were aligned to the reference genome using Hisat2, assembled with StringTie, and quantified with HTSeq. Differential gene expression analysis was conducted using edgeR with the following cutoff criteria: $|\log_2 FC| > 1$ and $P < 0.05$. Alternative splicing events were analyzed with rMATS. Gene enrichment analyses, including Gene Ontology and Kyoto Encyclopedia of Genes and Genomes pathway analyses, were performed using R packages from the Bioconductor platform (http://www.bioconductor.org/). Results were visualized on the Bioinforcloud online platform.

Reverse transcription quantitative real-time polymerase chain reaction (RT-qPCR)

The mRNA expression of target genes identified by RNA-seq was validated in both xenograft tumors and cultured CRPC cells. Total RNA was extracted, reverse transcribed into cDNA, and amplified using gene-specific primers (Sangon Biotech, China; sequences provided in **Table 1**). Amplification was performed on a Bio-Rad PCR system, and fluorescence was detected using an integrated RT-qPCR module. Relative gene expression levels were calculated using the 2-ΔΔCt method.

Immunofluorescence (IF)

Tumor tissues and cultured CRPC cells were fixed, paraffin-embedded, and sectioned. Following antigen retrieval and blocking, samples were incubated with primary antibodies (1:200 dilution) overnight at 4°C. After washing, fluorescent secondary antibodies and 4',6-diamidino-2-phenylindole were applied. Images were acquired using a fluorescence microscope.

Western blot

Protein expression in xenograft tumors and cultured CRPC cells were analyzed. Protein lysates (40 μg/μl) were quantified using a bicinchoninic acid assay, and 40 μg of total protein per sample was separated by sodium dodecyl sulfate-polyacrylamide gel electrophoresis and transferred onto polyvinylidene fluoride membranes. After blocking for 2-3 hours at room temperature, membranes were incubated overnight at 4°C with the following primary antibodies (all from Cell Signaling Technology, USA): phosphatidylinositol 3-kinase (PI3K) p85, protein kinase B (Akt), mechanistic target of rapamycin (mTOR), phospho-PI3K p85 (Tyr458), phospho-Akt (Ser473), phospho-mTOR (Ser2448), PGC1α, and glyceraldehyde-3-phosphate dehydrogenase. Following washing,

membranes were incubated with horseradish peroxidase-conjugated secondary antibodies. Signals were detected using a chemiluminescent imaging system (Bio-Rad, USA) and quantified with Image J software (National Institutes of Health, USA).

Statistical analysis

Data are expressed as mean ± standard error of the mean. Normality and homogeneity of variance were assessed using the Shapiro-Wilk test and Levene's test, respectively. Comparisons between two groups were performed using Student's t-test (for equal variances) or Welch's t-test (for unequal variances). Multi-group comparisons were conducted by one-way analysis of variance followed by Tukey's post-hoc test (for homogeneous variances) or Welch's analysis of variance followed by Games-Howell post-hoc test (for heterogeneous variances). A *P*-value <0.05 was considered statistically significant. All statistical analyses and graphs were generated using GraphPad Prism version 9.0.0.

Results

PLP-containing serum exerts broad anti-tumor activity against CRPC cells in vitro

To determine the appropriate experimental concentration, we first assessed the cytotoxicity of PLP-containing serum, which was prepared from rats orally administered PLP. In the androgen-independent prostate cancer cell lines PC-3 and 22RV1, CCK-8 assays showed that the serum reduced cell viability in a concentration-dependent manner. The inhibitory effect increased progressively from 0% to 30% serum concentration and then stabilized (**Figure 1A**) at 30% concentration, viability decreased to 24.00% in PC-3 cells and 31.89% in 22RV1 cells (P<0.001 vs. control), establishing this concentration as the maximum inhibitory threshold for subsequent experiments. Consistent with this, SRB-based proliferation assays confirmed sustained inhibition under treatment with 30% PLP-containing serum (**Figure 1C**). Beyond proliferation, functional phenotyping revealed that the same treatment significantly reduced wound closure in scratch assays (**Figure 1B**), inhibited Matrigel invasion in Transwell assays (**Figure 1D**), and increased both early and late apoptosis as shown by Annexin V/PI staining (**Figure 1E**). Notably, although castration-resistant progression is often associated with elevated intercellular ROS, PLP exposure sharply reduced ROS levels, as detected by 2',7'-dichlorodihydrofluorescein diacetate fluorescence (**Figure 1F**). Collectively, these data indicate that PLP-containing serum simultaneously targets multiple hallmarks of CRPC, including proliferation, migration, invasion, survival, and redox imbalance. These findings provide a solid foundation for further mechanistic investigation.

Purified PLP recapitulates the anti-CRPC activity observed with PLP-containing serum

To determine whether the observed effects were specifically attributable to PLP itself rather than serum metabolites or nonspecific factors, we directly treated PC-3 and 22RV1 cells with highly purified PLP (>95% purity). Purified PLP alone robustly reproduced all key antitumor phenotypes observed with the serum formulation: it significantly inhibited wound healing (**Figure 2A**), reduced Matrigel invasion (**Figure 2B**), induced pronounced apoptosis (**Figure 2C**), and markedly lowered intracellular ROS levels (**Figure 2D**). The magnitude of these effects was comparable to that achieved with 30% PLP-containing serum. These results demonstrate that PLP is the primary bioactive component responsible for the antitumor activity, confirming the specificity of our model and supporting its potential applicability as a targeted therapeutic agent.

PLP suppresses CRPC tumor growth in vivo with good safety profile

We next evaluated the in vivo efficacy of orally administered PLP using a castrated PC-3 xenograft model. After 28 days of treatment, PLP caused a dose-dependent reduction in both tumor volume and weight. The high-dose group (400 mg/kg) showed a 91.7% decrease in tumor volume and a 78.0% decrease in tumor weight compared to the vehicle control (P<0.001), achieving efficacy comparable to the clinical combination of abiraterone and prednisone (97.4% inhibition) (**Figure 3A-C**). Histopathological examination of excised tumors revealed extensive apoptotic regions in the PLP-treated groups, particularly at the high dose (**Figure 3D**). Serum levels of creatinine, urea nitrogen, alanine aminotransferase, and

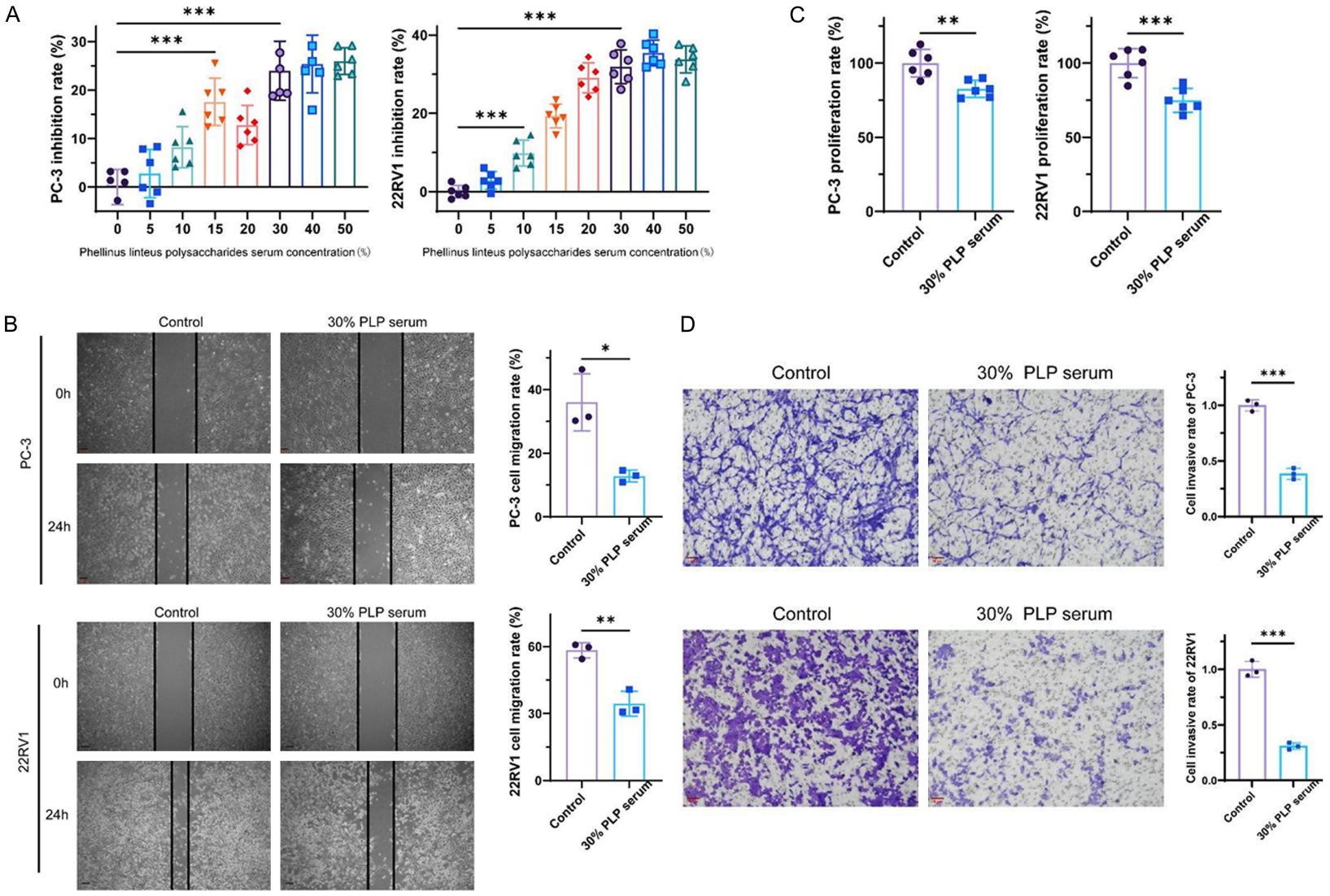
A
PC-3 inhibition rate (%)
22RV1 inhibition rate (%)
Phellinus linteus polysaccharides serum concentration (%)
Phellinus linteus polysaccharides serum concentration (%)
C
PC-3 proliferation rate (%)
22RV1 proliferation rate (%)
Control
30% PLP serum
B
Control
30% PLP serum
PC-3
22RV1
0h
24h
PC-3 cell migration rate (%)
22RV1 cell migration rate (%)
D
Control
30% PLP serum
Cell invasive rate of PC-3
Cell invasive rate of 22RV1

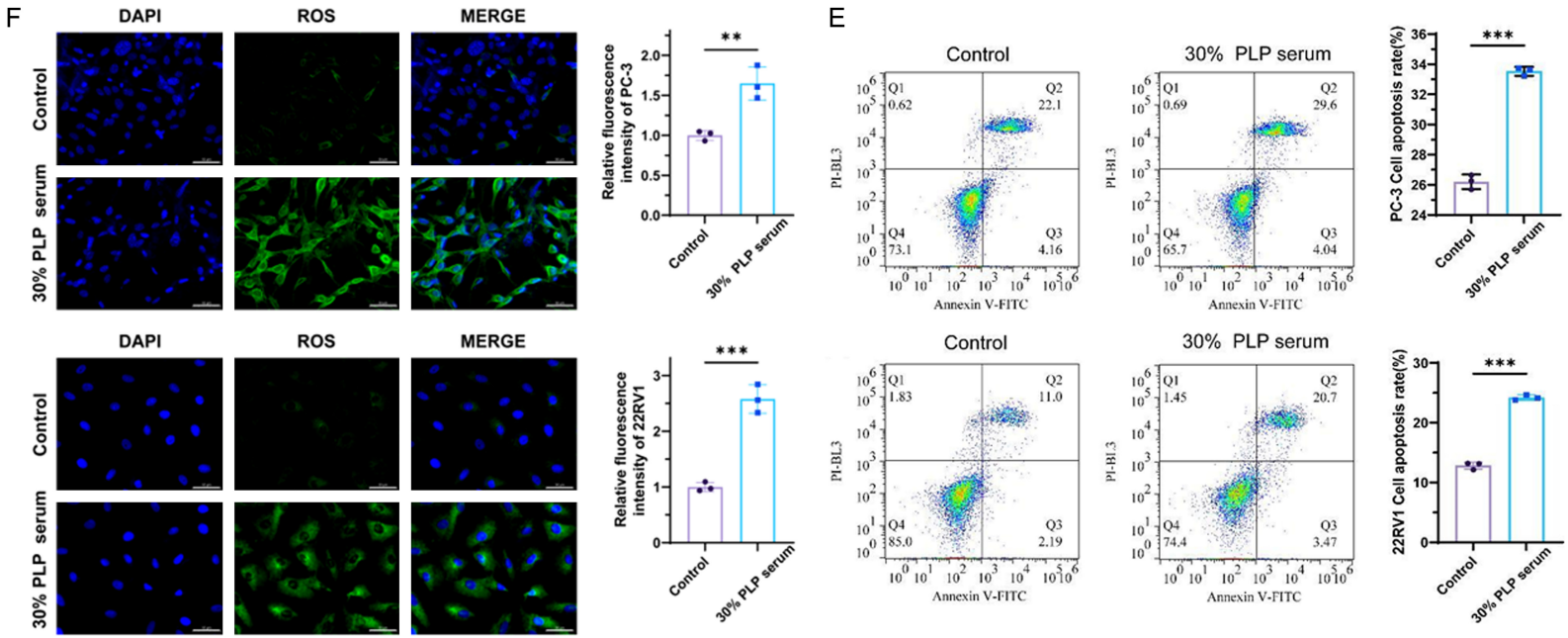

Figure 1. In vitro effects of PLP-containing serum on CRPC cells. PC-3 and 22RV1 cells were treated with rat serum containing PLP at the indicated concentrations for 48 h. A. Cell viability assessed by CCK-8 assay. B. Cell migration evaluated by wound healing assay. Scale bar: 200 μm. C. Cell proliferation measured by SRB assay. D. Cell invasion determined by Transwell assay with Matrigel coating. Scale bar: 100 μm. E. Apoptosis analyzed by Annexin V/PI double staining and flow cytometry. F. Intracellular ROS levels detected by DCFH-DA fluorescence. Scale bar: 50 μm. Data are presented as mean ± SD of three independent experiments. *P<0.05, **P<0.01, ***P<0.001. PLP, *Phellinus linteus* polysaccharides; CRPC, castration-resistant prostate cancer; DAPI, 4',6-diamidino-2-phenylindole; ROS, reactive oxygen species; Annexin V-FITC, Annexin V-fluorescein isothiocyanate; CCK-8, Cell Counting Kit-8; SRB, sulforhodamine B; Annexin V/PI, Annexin V-fluorescein isothiocyanate/propidium iodide; DCFH-DA, 2',7'-dichlorodihydrofluorescein diacetate; SD, standard deviation.

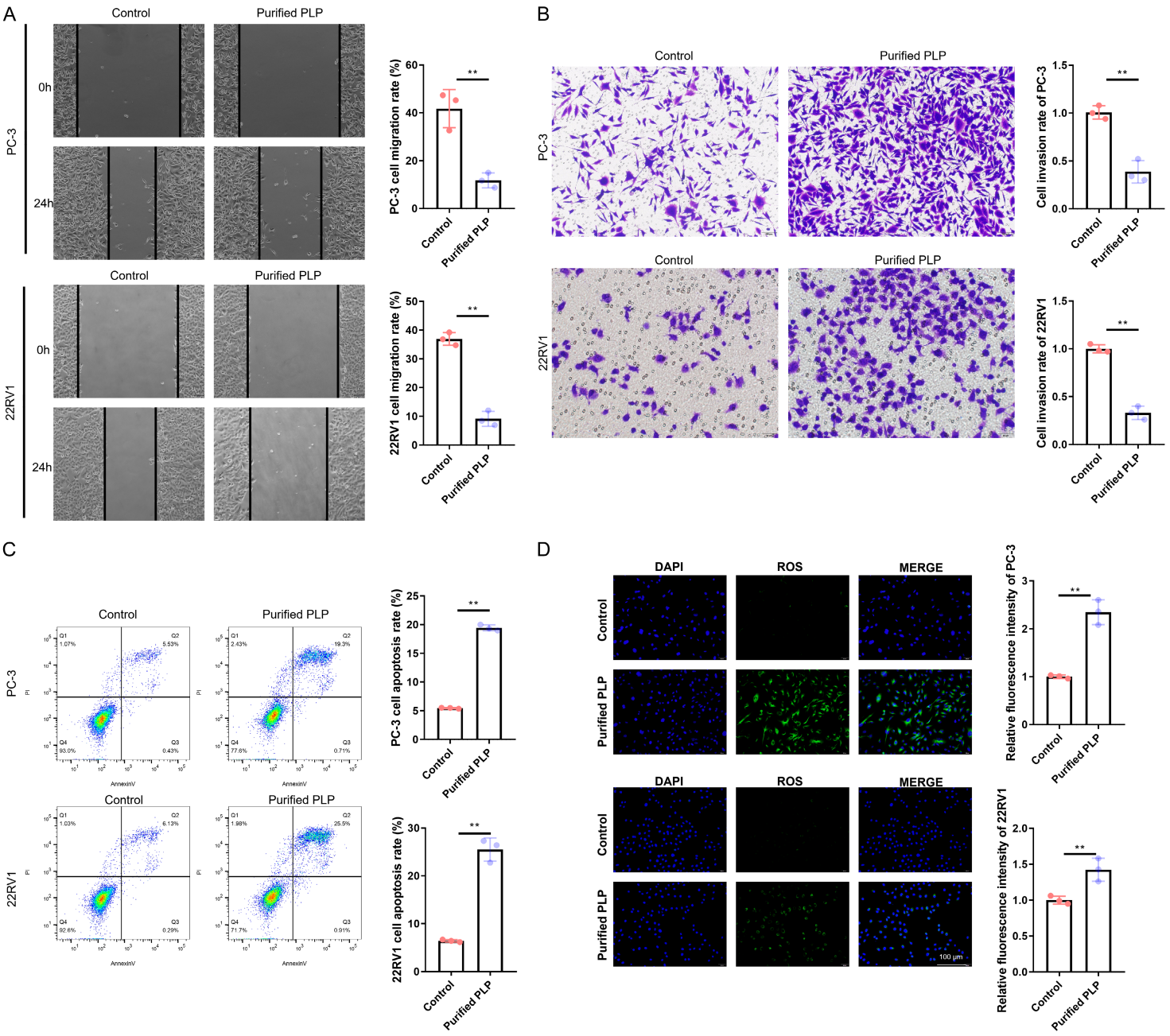
A
Control
Purified PLP
PC-3
0h
24h
22RV1
PC-3 cell migration rate (%)
22RV1 cell migration rate (%)
B
Cell invasion rate of PC-3
Cell invasion rate of 22RV1
C
PC-3 cell apoptosis rate (%)
22RV1 cell apoptosis rate (%)
D
DAPI
ROS
MERGE
Relative fluorescence intensity of PC-3
Relative fluorescence intensity of 22RV1
100 μm

Figure 2. Phenotypic effects of purified PLP on CRPC cells. PC-3 and 22RV1 cells were treated with purified PLP (50 μg/mL) for 48 h. A. Cell migration assessed by wound healing assay. Scale bar: 200 μm. B. Cell invasion evaluated by Matrigel-based Transwell assay. Scale bar: 100 μm. C. Apoptosis analyzed by Annexin V/PI double staining and flow cytometry. D. Intracellular ROS levels detected using DCFH-DA fluorescent probe. Scale bar: 50 μm. Data are presented as mean ± SD from three independent experiments. *P<0.05, **P<0.01, ***P<0.001. PLP, *Phellinus linteus* polysaccharides; CRPC, castration-resistant prostate cancer; DAPI, 4',6-diamidino-2-phenylindole; ROS, reactive oxygen species; Annexin V/PI, Annexin V-fluorescein isothiocyanate/propidium iodide; DCFH-DA, 2',7'-dichlorodihydrofluorescein diacetate; SD, standard deviation.

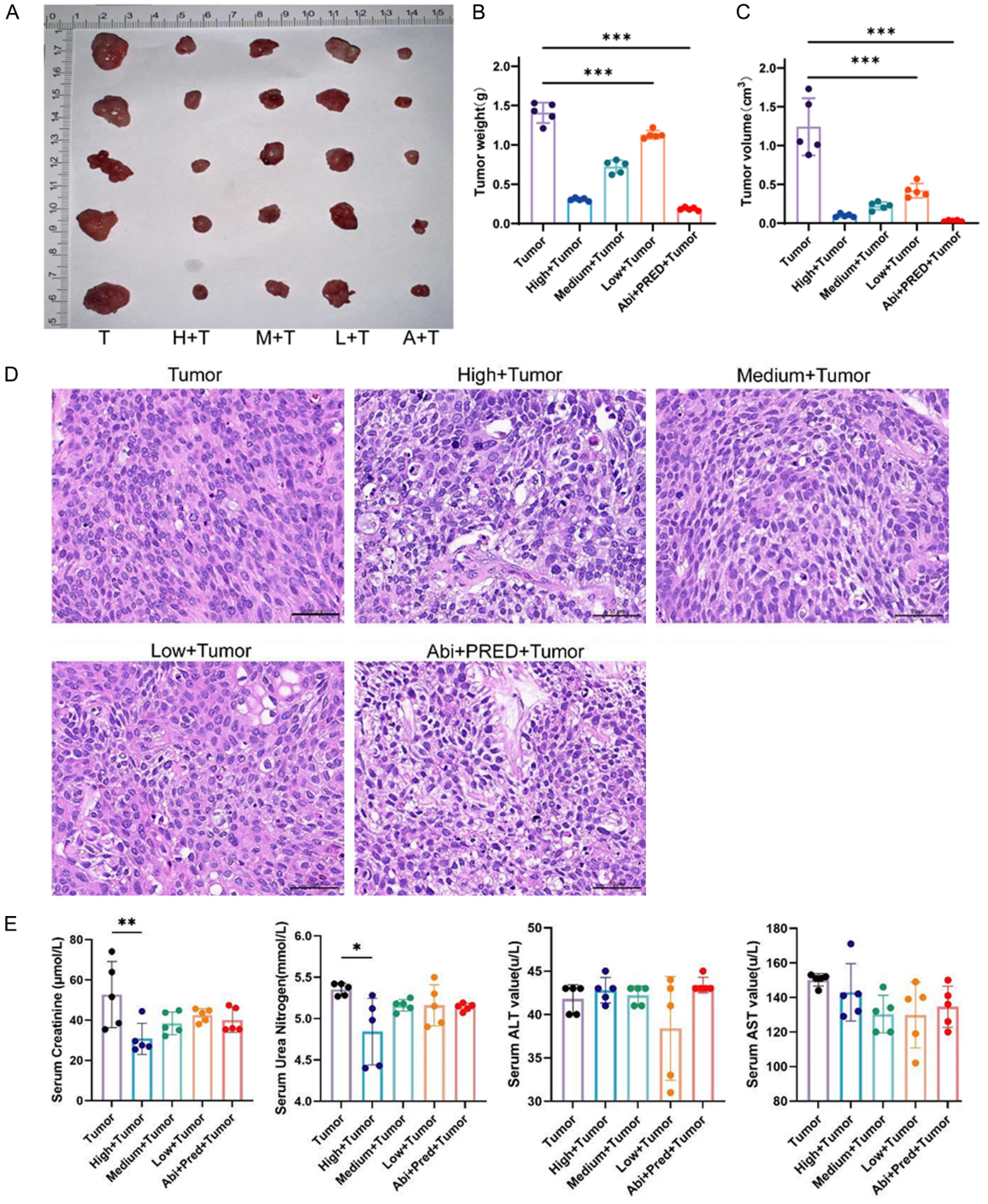

Figure 3. In vivo anti-tumor efficacy and safety of PLP in a CRPC xenograft model. Castrated nude mice bearing PC-3 xenografts were orally administered vehicle, PLP (100, 200, or 400 mg/kg), or abiraterone/prednisone daily for 28

days (n=6 per group). A. Tumor volume was measured every 3-4 days. B. Tumors were excised and weighed at the endpoint. C. Tumor inhibition rate was calculated relative to the vehicle group. D. Representative H&E-stained tumor sections. Scale bar: 100 μm. E. Serum levels of creatinine, urea nitrogen, ALT, and AST were measured to assess hepatorenal function. *P<0.05, **P<0.01, ***P<0.001. PLP, *Phellinus linteus* polysaccharides; CRPC, castration-resistant prostate cancer; H&E, hematoxylin and eosin; T, tumor (vehicle control); H+T, high-dose PLP (400 mg/kg) + tumor; M+T, medium-dose PLP (200 mg/kg) + tumor; L+T, low-dose PLP (100 mg/kg) + tumor; A+T, abiraterone (130 mg/kg) + prednisone (1.3 mg/kg) + tumor; Abi + PRED, abiraterone + prednisone; ALT, alanine aminotransferase; AST, aspartate aminotransferase.

aspartate aminotransferase remained within normal ranges across all treatment groups (**Figure 3E**), indicating no significant hepatotoxicity or nephrotoxicity. These preclinical results establish PLP as a potent and safe anti-CRPC agent.

Transcriptomic profiling identifies Phosphoinositide-3-kinase regulatory subunit 1 (PIK3R1) downregulation and PGC-1α upregulation as hallmarks of PLP response in CRPC

To elucidate the molecular mechanisms of PLP's anti-tumor activity, RNA-Seq was performed on tumor samples from castrated nude mice bearing PC-3 xenografts treated with vehicle control, low-dose PLP (L+T), medium-dose PLP (M+T), high-dose PLP (H+T), or abiraterone/prednisone (A+T). After applying stringent filtering criteria ($|\log_2$ fold change$|$ >1, adjusted P<0.05), a core set of 85 differentially expressed genes was identified that showed consistent alteration across all relevant pairwise comparisons (H+T vs. control, M+T vs. control, H+T vs. L+T), excluding repeat and dose-irrelevant hits.

Gene Ontology enrichment analysis highlighted biological pathways related to "phosphatidylinositol-mediated signaling", "regulation of cell migration", and "response to oxidative stress". Kyoto Encyclopedia of Genes and Genomes pathway analysis revealed that the most significantly down-regulated oncogenic pathway was the PI3K-Akt signaling pathway (P<0.001, **Figure 4A**). Within this pathway, *PIK3R1* (encoding the p85α regulatory subunit), which stabilizes and modulates PI3K catalytic activity, emerged as the most down-regulated gene across all effective treatment groups (**Figure 4B**).

In parallel, we observed pronounced up-regulation of genes involved in mitochondrial function and oxidative stress defense. PPARGC1A, the gene encoding PGC-1α - a master transcriptional coactivator regulating mitochondrial biogenesis, ROS detoxification, and metabolic adaptation-was among the most consistently up-regulated transcripts. This dual signature, combining suppression of PI3K activity with PGC-1α-mediated redox homeostasis, was further validated by cross-referencing our list of differentially expressed genes with a curated set of CRPC-related protein-coding genes from the GeneCards Database. Among the seven overlapping targets, PIK3R1 and PPARGC1A were the most striking, exhibiting opposite expression trends and both playing established roles in cancer progression and therapy resistance (**Figure 4C**).

PLP co-suppresses the PI3K-Akt-mTOR oncogenic pathway and upregulates PGC-1α in CRPC in vitro and in vivo

To delineate the molecular changes induced by PLP treatment, we performed integrated transcriptomic and proteomic analyses in both xenograft tumors and cultured CRPC cells. RT-qPCR analysis of xenograft tumors revealed that PLP administration dose-dependently reduced mRNA expression of PIK3R1 (the regulatory subunit of PI3K) and its downstream effectors Akt and mTOR, while upregulating PGC-1α, a master regulator of mitochondrial function and oxidative stress response (**Figure 5A**). A similar suppression of PIK3R1 mRNA was observed in PC-3 and 22RV1 cells treated with PLP-containing serum (**Figure 5B**). At the protein level, immunofluorescence staining of tumor sections showed marked reductions in cytoplasmic PIK3R1, phosphorylated Akt (Ser473), and phosphorlated mTOR (Ser2448), alongside a clear increase in nuclear PGC-1α fluorescence(**Figure 5C**). These changes were recapitulated in cultured cells, where PLP significantly decreased PIK3R1 protein levels in both cell lines (**Figure 5D**). Western blotting further confirmed that PLP reduced the phosphorylation of PIK3R1, Akt, and mTOR without altering total protein levels, indicating specific inhi-

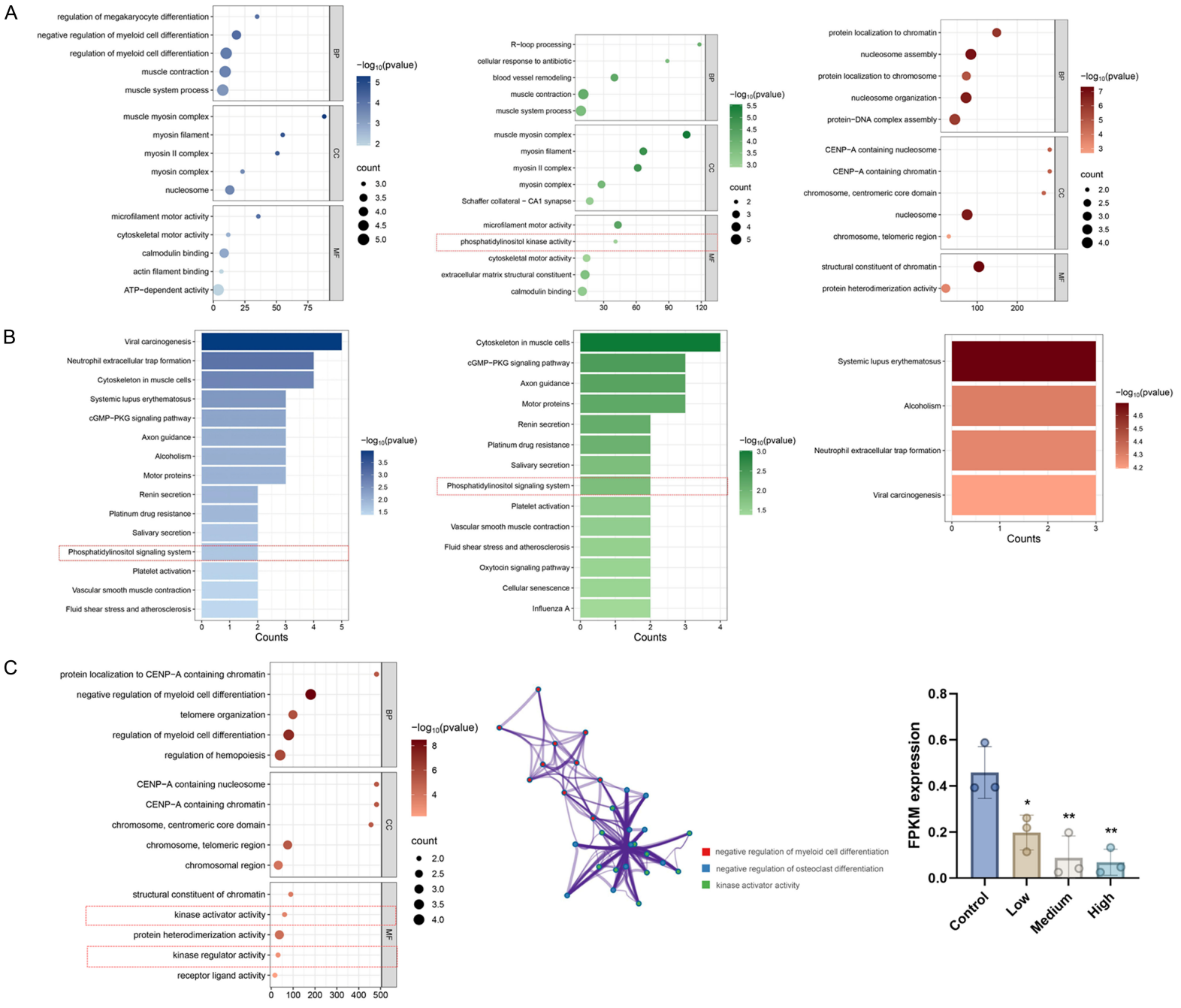
A
regulation of megakaryocyte differentiation
negative regulation of myeloid cell differentiation
regulation of myeloid cell differentiation
muscle contraction
muscle system process
muscle myosin complex
myosin filament
myosin II complex
myosin complex
nucleosome
microfilament motor activity
cytoskeletal motor activity
calmodulin binding
actin filament binding
ATP-dependent activity
BP
CC
MF
−log10(pvalue)
count
R-loop processing
cellular response to antibiotic
blood vessel remodeling
Schaffer collateral − CA1 synapse
phosphatidylinositol kinase activity
extracellular matrix structural constituent
protein localization to chromatin
nucleosome assembly
protein localization to chromosome
nucleosome organization
protein-DNA complex assembly
CENP-A containing nucleosome
CENP-A containing chromatin
chromosome, centromeric core domain
chromosome, telomeric region
structural constituent of chromatin
protein heterodimerization activity
B
Viral carcinogenesis
Neutrophil extracellular trap formation
Cytoskeleton in muscle cells
Systemic lupus erythematosus
cGMP-PKG signaling pathway
Axon guidance
Alcoholism
Motor proteins
Renin secretion
Platinum drug resistance
Salivary secretion
Phosphatidylinositol signaling system
Platelet activation
Vascular smooth muscle contraction
Fluid shear stress and atherosclerosis
Oxytocin signaling pathway
Cellular senescence
Influenza A
Counts
C
protein localization to CENP-A containing chromatin
negative regulation of myeloid cell differentiation
telomere organization
regulation of myeloid cell differentiation
regulation of hemopoiesis
chromosomal region
kinase activator activity
protein heterodimerization activity
kinase regulator activity
receptor ligand activity
negative regulation of osteoclast differentiation
FPKM expression
Control
Low
Medium
High

Figure 4. Transcriptomic profiling of PLP-treated CRPC xenograft tumors. RNA sequencing was performed on tumor tissues from castrated nude mice bearing PC-3 xenografts after 28 days of oral treatment with vehicle or PLP (100-400 mg/kg). A. KEGG pathway enrichment analysis of differentially expressed genes ($|\log_2 FC| > 1$, adjusted $P<0.05$). B. GO biological process enrichment analysis of differentially expressed genes ($|\log_2 FC| > 1$, adjusted $P<0.05$). C. Overlap of differentially expressed genes with curated CRPC-associated gene sets. *P<0.05, **P<0.01, ***P<0.001. PLP, *Phellinus linteus* polysaccharides; CRPC, castration-resistant prostate cancer; KEGG, Kyoto Encyclopedia of Genes and Genomes; $\log_2 FC$, $\log_2$ fold change; ATP, adenosine triphosphate; GO, Gene Ontology; CENP-A, centromere protein A; cGMP-PKG, cyclic guanosine monophosphate-protein kinase G; FPKM, fragments per kilobase of transcript per million mapped reads.

bition of pathway activation. Concurrently, PGC-1α protein was upregulated. These alterations were evident in both tumor lysates (**Figure 5E**) and lysates from the two CRPC cell lines (**Figure 5F**). Collectively, these multi-omics data demonstrate that PLP exerts its anti-tumor effects through a dual mechanism: simultaneous suppression of the oncogenic PI3K-Akt-mTOR signaling cascade and activation of the PGC-1α-driven antioxidant and metabolic adaptation program, thereby linking phenotypic suppression to coherent molecular reprogramming.

PIK3R1 overexpression functionally rescues PLP-induced tumor suppression

To establish a causal relationship between PIK3R1 downregulation and the phenotypic effects of PLP, we generated 22RV1 cells stably overexpressing PIK3R1 via pcDNA3.1-based transfection. In vector-control cells, PLP treatment robustly inhibited migration (**Figure 6A**), invasion (**Figure 6B**), induced apoptosis (**Figure 6C**), and reduced ROS levels (**Figure 6D**)-fully consistent with prior observations. In contrast, forced expression of PIK3R1 significantly reversed all these phenotypes: wound closure and Transwell invasion were partially restored, apoptosis induction was blunted, and the PLP-mediated decline in ROS was attenuated. These rescue experiments provide direct functional evidence that suppression of PIK3R1 is necessary for PLP to exert its anti-CRPC activity, positioning it as a critical node in the PLP response network.

PGC-1α knockdown abrogates PLP's redox-modulating and anti-tumor effects

Conversely, to determine the functional contribution of PGC-1α, we silenced its expression in 22RV1 cells using lentiviral shRNA. In PGC-1α-knockdown cells, PLP failed to effectively suppress migration (**Figure 7A**) and invasion (**Figure 7B**), induced significantly less apoptosis (**Figure 7C**), and no longer reduced intracellular ROS levels to the same extent as in control shRNA-treated cells (**Figure 7D**). This loss-of-function validation confirms that PGC-1α is indispensable for mediating PLP's antioxidant and tumor-suppressive actions. Together with the PIK3R1 rescue data, these findings establish a unified model in which PLP combats CRPC through dual modulation of oncogenic signaling and metabolic-redox adaptation.

Discussion

Hormone-sensitive prostate cancer progresses to CRPC through a complex pathological process involving both androgen receptor (AR)-dependent and AR-independent mechanisms [11, 12]. This transition is characterized by diverse molecular alterations, necessitating a comprehensive understanding of the tumor across disease stages. While early-stage prostate cancer can often be effectively managed with options such as surgery, radiation, or androgen deprivation therapy, treatment becomes increasingly challenging once the disease progresses to CRPC. In this context, botanical medicines may represent a promising therapeutic breakthrough.

Multiple studies have reported the anti-prostate cancer effects of *P. linteus* extracts, which primarily consist of polysaccharides. High doses of PLP have been shown to activate caspase-2, caspase-8, and endoplasmic reticulum stress-related apoptotic pathways, thereby promoting apoptosis in the Lymph Node Carcinoma of the Prostate cell line [12]. In murine tumor models, Sanghuang extract has been found to influence the incidence and progression of tumors formed by PC-3 or DU145 prostate cancer cells, with apoptosis mediated through caspase-3 activation [13, 14]. Additionally, studies suggest that the anti-cancer mechanism of Sanghuang extract involves downregulation of phosphorylated sig-

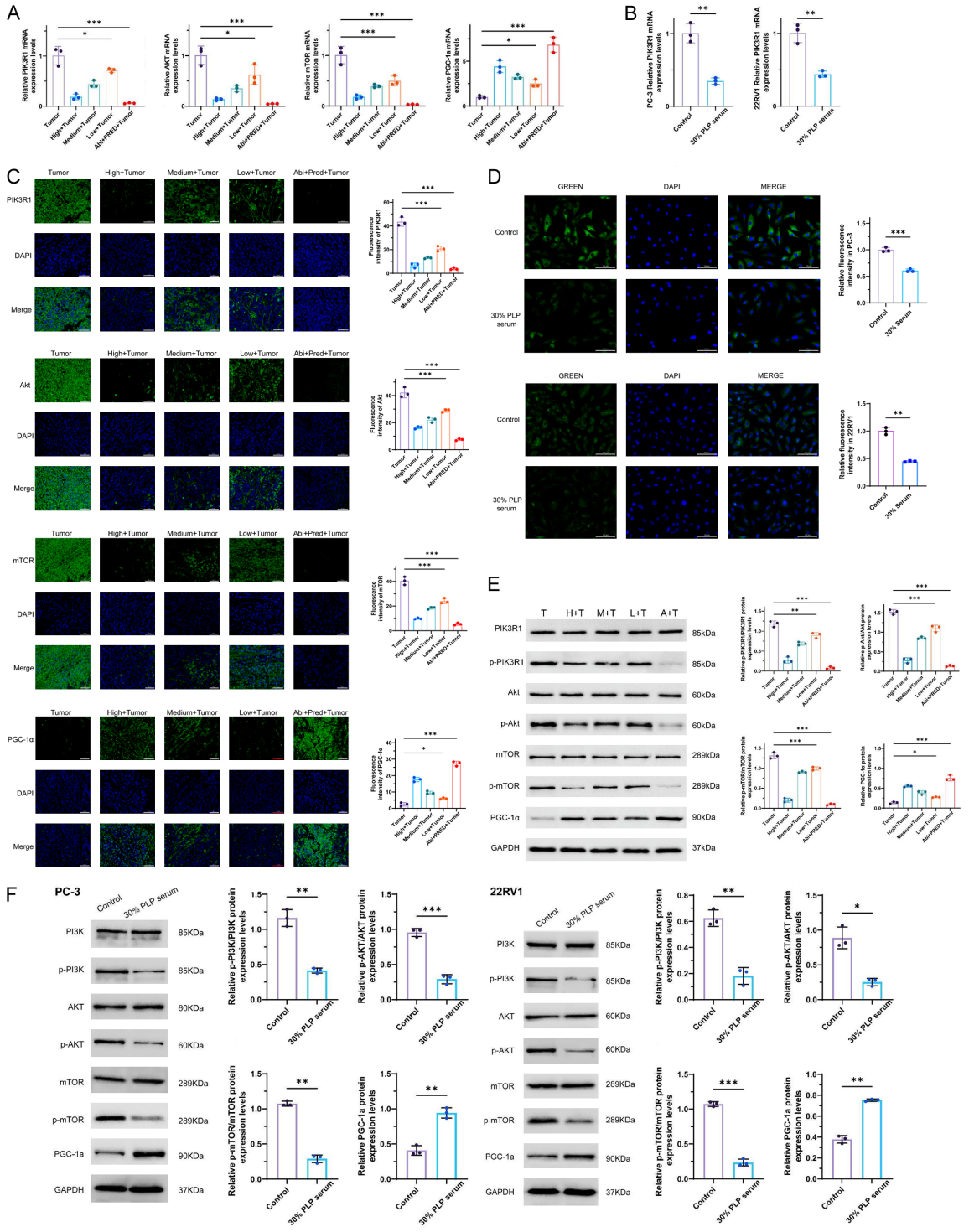

Figure 5. Molecular characterization of PI3K-Akt-mTOR and PGC-1α signaling in response to PLP. A. RT-qPCR analysis of PIK3R1, Akt, mTOR, and PGC-1α mRNA levels in xenograft tumor tissues. B. RT-qPCR of PIK3R1 mRNA in PC-3 and 22RV1 cells treated with 30% PLP-containing serum. C. Immunofluorescence staining of PIK3R1, p-Akt (Ser473), p-mTOR (Ser2448), and PGC-1α in tumor sections. Scale bar: 50 μm. D. Immunofluorescence of PIK3R1 in PC-3 and 22RV1 cells. Scale bar: 25 μm. E. Western blot analysis of p-PIK3R1, total PIK3R1, p-Akt, total Akt, p-mTOR, total mTOR, PGC-1α, and β-actin in tumor lysates. F. Western blot of the same proteins in PC-3 and 22RV1 cell lysates. β-actin was used as a loading control. *P<0.05, **P<0.01, ***P<0.001. PIK3R1, phosphoinositide-3-kinase regulatory subunit 1; Abi + PRED, abiraterone + prednisone; Akt, protein kinase B; mTOR, mechanistic target of rapamycin; PGC-1α, peroxisome proliferator-activated receptor gamma coactivator 1-alpha; PLP, *Phellinus*

linteus polysaccharides; DAPI, 4',6-diamidino-2-phenylindole; T, tumor (vehicle control); H+T, high-dose PLP (400 mg/kg) + tumor; M+T, medium-dose PLP (200 mg/kg) + tumor; L+T, low-dose PLP (100 mg/kg) + tumor; A+T, abiraterone (130 mg/kg) + prednisone (1.3 mg/kg) + tumor; p-PIK3R1, phosphorylated phosphoinositide-3-kinase regulatory subunit 1; p-Akt, phosphorylated protein kinase B; p-mTOR, phosphorylated mechanistic target of rapamycin; GAPDH, glyceraldehyde-3-phosphate dehydrogenase; RT-qPCR, Quantitative reverse transcription polymerase chain reaction.

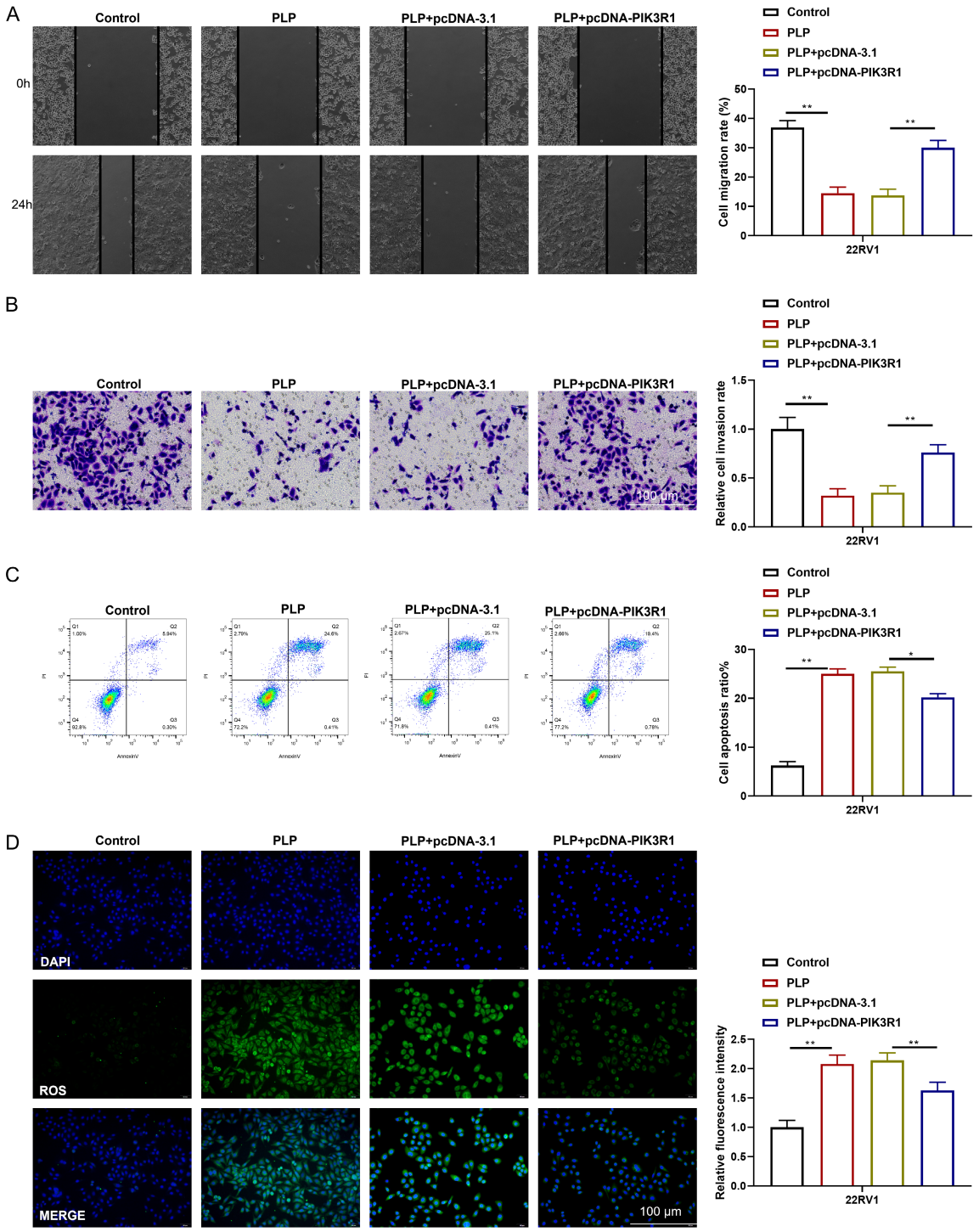

Figure 6. Functional rescue by PIK3R1 overexpression in 22RV1 cells. 22RV1 cells were transfected with pcDNA3.1-PIK3R1 or empty vector, followed by PLP treatment. A. Wound healing assay. Scale bar: 200 μm. B. Transwell

invasion assay with Matrigel coating. Scale bar: 100 μm. C. Apoptosis analyzed by Annexin V/PI staining and flow cytometry. D. Intracellular ROS levels detected using DCFH-DA. Scale bar: 50 μm. Data are representative of three independent experiments. *P<0.05, **P<0.01, ***P<0.001. PLP, *Phellinus linteus* polysaccharides; PIK3R1, phosphoinositide-3-kinase regulatory subunit 1; DAPI, 4',6-diamidino-2-phenylindole; ROS, reactive oxygen species; Annexin V/PI, Annexin V-fluorescein isothiocyanate/propidium iodide; DCFH-DA, 2',7'-dichlorodihydrofluorescein diacetate.

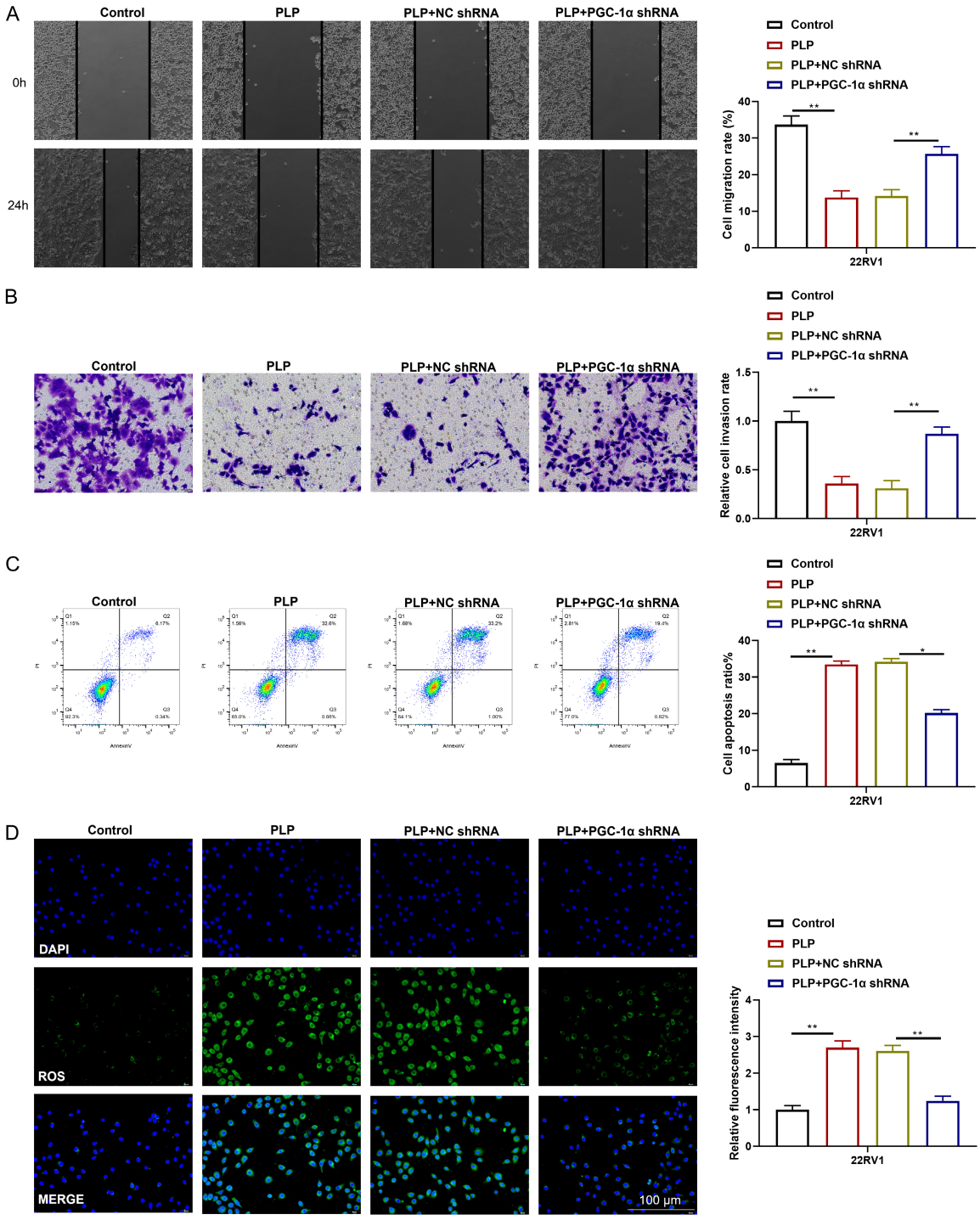

Figure 7. Effects of PGC-1α knockdown on PLP responsiveness in 22RV1 cells. 22RV1 cells were infected with lentivirus expressing shRNA targeting PGC-1α or a non-targeting control, followed by treatment with PLP. A. Wound heal-

ing assay. Scale bar: 200 μm. B. Matrigel-based Transwell invasion assay. Scale bar: 100 μm. C. Apoptosis analyzed by Annexin V/PI staining and flow cytometry. D. Intracellular ROS levels measured using DCFH-DA fluorescence. Scale bar: 50 μm. Data are representative of three independent experiments. *P<0.05, **P<0.01, ***P<0.001. PLP, *Phellinus linteus* polysaccharides; NC shRNA, non-targeting control shRNA; PGC-1α, peroxisome proliferator-activated receptor gamma coactivator 1-alpha; DAPI, 4',6-diamidino-2-phenylindole; ROS, reactive oxygen species; Annexin V/PI, Annexin V-fluorescein isothiocyanate/propidium iodide; DCFH-DA, 2',7'-dichlorodihydrofluorescein diacetate.

nal transducer and activator of transcription 3, leading to apoptosis via mitochondrial pathways [15]. Other researchers have demonstrated that two main polysaccharide components of Sanghuang (*P. linteus* Ethanol-soluble fraction and *P. linteus* Iodine-identified Ethanol-soluble fraction) exhibit anti-cancer activity against ten cancer cell types, including prostate cancer, accompanied by significant activation of pro-apoptotic factors such as caspase-3 and caspase-9, which were attributed to oxidative stress and its link to apoptosis [16]. However, research specifically on focusing on high-purity PLP in the context of CRPC remains limited. Given that PLP may share similar bioactive properties, we selected the aforementioned in vitro celluar endpoints for investigation. The results of ROS detection further suggest a potential association between PLP and the PGC-1α gene.

In this study, we selected two representative CRPC cell lines: PC-3 and 22RV1. While these lines share fundamental biological characteristics and metabolic pathways, they may exhibit subtle differences in nutrient utilization, proliferation, and gene expression profiles. The consistent anti-tumor effects observed across both lines suggest that PLP's activity is likely robust and broadly applicable. PLP is a heteropolysaccharide primarily composed of glucose along with other monosaccharides. Its composition aligns with previously reported polysaccharide profiles from *Phellinus* species [17]. The PLP used herein was obtained as a polysaccharide preparation (≥90% purity) from a reputable biotechnology supplier. It was prepared via hot-water extraction, ethanol precipitation after concentration, deproteinization using the Sevag method, and chromatographic purification. Although *P. linteus* is a natural product and minor batch-to-batch variations may occur, the standardized preparation protocol ensures reproducible experimental outcomes.

Following PLP treatment, intracellular ROS levels decreased, while the rate of cell death increased. This indicates that PLP does not induce cell death through oxidative stress, a conclusion consistent with previous reports on the antioxidant properties of PLP [18].

Currently available animal studies report an exploratory oral dosage range for PLP of 100-1000 mg/kg, with optimal therapeutic effects generally observed between 200-500 mg/kg [13]. Accordingly, in our nude mouse experiment, we selected high (400 mg/kg), intermediate (200 mg/kg), and low (100 mg/kg) dose levels. Oral administration of PLP at these doses or vehicle control to nude mice bearing subcutaneous human CRPC xenografts demonstrated clear anti-tumor effects at both macroscopic and microscopic levels. Although no comprehensive toxicological analysis was performed, routine examination revealed no obvious signs of hepatotoxicity or nephrotoxicity.

RNA sequencing of tumor tissues revealed that PLP downregulated PIK3R1 expression. This finding was functionally validated, as PLP was shown to inhibit the phosphorylation of PIK3R1 and its downstream effectors Akt and mTOR, thereby contributing to its anti-cancer activity. The PI3K/Akt/mTOR pathway plays a well-established role in disease progression, therapeutic resistance, and metastasis in metastatic CRPC. PIK3R1 encodes the p85α regulatory subunit of PI3K, while p85β and p55γ are encoded by PIK3R2 and PIK3R3, respectively [19, 20]. The role of PIK3R1 in cancer appears context-dependent. In some models, PIK3R1 deletion promotes tumorigenesis-for instance, driving invasive liver tumors in mice [21] or exacerbating epithelial tumor formation in PTEN-deficient backgrounds, with heterozygous loss increasing colonic polyp number [22]. Similarly, PIK3R1 loss has been linked to enhanced malignancy in breast cancer cells and mouse models [23, 24]. Conversely, clinical evidence from breast can-

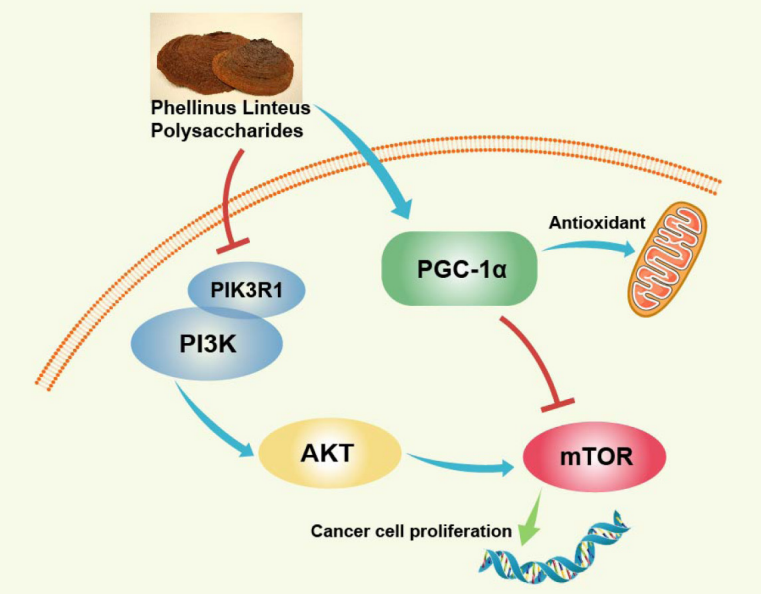

Figure 8. Mechanistic overview of PLP in tumor suppression. PI3K, phosphoinositide 3-kinase; PIK3R1, phosphoinositide-3-kinase regulatory subunit 1; PGR-1α, peroxisome proliferator-activated receptor gamma coactivator 1-alpha; mTOR, mechanistic target of rapamycin.

cer indicates that elevated PIK3R1 expression in approximately 31% of tumor samples correlates with metastasis and poorer survival [25]. In liver cancer, PIK3R1 is upregulated compared to adjacent normal tissue, and its silencing suppresses phosphorylation of PI3K, Akt, and mTOR, exerting anti-tumor effects in hepatocellular carcinoma cell lines [26]. Although in vitro silencing of PIK3R1 or related genes generally inhibits proliferation, invasion, and migration, the magnitude and mechanism of response can vary across cell lines due to distinct signaling network configurations [27]. These observations underscore the complex, tissue-specific regulation of PIK3R1.

In CRPC, AR signaling becomes dysregulated, and oncogenic PI3K/Akt/mTOR activation frequently coexists. Approximately 15-30% of CRPC cases harbor PIK3CA amplification or mutation [28, 29], leading to constitutive Akt activation that sustains cancer cell survival, proliferation, and metabolic reprogramming [30]. Normally, PI3K/Akt/mTOR and AR signaling engage in reciprocal feedback; inhibition of one pathway often activates the other. In CRPC, adaptive changes in the AR pathway-such as AR amplification, mutation, or expression of splice variants like AR-V7-enable tumors to bypass androgen deprivation [31, 32]. Consequently, CRPC cells frequently develop heightened dependence on PI3K/Akt/mTOR signaling, making this pathway a rational therapeutic target alongside androgen deprivation [33].

PGC-1α is a key transcriptional coactivator that regulates metabolism, mitochondrial biogenesis, and oxidative stress responses. Its role in cancer can be dual, promoting or suppressing tumor progression depending on tumor type and microenvironment. It may help protect against oxidative DNA damage and reduce cancer risk [34]. The PI3K/Akt/mTOR pathway and PGC-1α are interconnected in tumor development. PI3K/Akt/mTOR signaling promotes glycolysis through transcription factors such as hypoxia-inducible factor 1-alpha and Myc, supporting the Warburg effect and tumor growth. In contrast, PGC-1α enhances mitochondrial oxidative phosphorylation and suppresses glycolysis, counteracting the metabolic shift driven by PI3K/Akt/mTOR [35]. Additionally, mechanistic target of rapamycin complex 1-activated ribosomal protein S6 kinase 1 can inhibit autophagy and mitochondrial turnover, impairing PGC-1α function and facilitating metabolic adaptation in cancer cells. PGC-1α also interacts with the Wnt/β-catenin and PI3K/Akt pathways, contributing to reduced tumor stemness and metastasis [36]. In this study, PLP upregulated PGC-1α expression, suggesting a potential link to PI3K/Akt/mTOR pathway modulation (**Figure 8**).

Safety evaluation in this study was limited to serum markers of hepatic and renal function. Comprehensive toxicology assessments-including organ weight indices, full histopathology of major organs, and systemic inflammatory profiling-were not conducted. Such analyses will be important for future chronic toxicity studies supporting Investigational New Drug application. Although PLP robustly inhibited migration and invasion in vitro, the subcutaneous xenograft model does not replicate meta-

static progression. Future studies should employ orthotopic prostate implantation, intracardiac injection, or patient-derived circulating tumor cell models to evaluate PLP's potential anti-metastatic effects. Furthermore, while tumor growth suppression and apoptosis were observed via Hematoxylin and Eosin as well as Terminal Deoxynucleotidyl Transferase dUTP Nick-End Labeling, additional immunohistochemical analyses (e.g., Ki-67 for proliferation and cleaved caspase-3 for apoptosis) would strengthen in vivo phenotyping. These were not feasible in the current study due to limited residual tissue after molecular analyses but are planned for follow-up investigations.

In conclusion, PLP exhibits certain inhibitory effects on the progression of CRPC in both in vitro assays and xenograft animal models. The mechanism of action likely involves downregulation of the PI3K/Akt/mTOR oncogenic signaling pathway and the synergistic antioxidant effects associated with PGC-1α upregulation. These findings provide a solid scientific foundation supporting PLP as a promising candidate for anti-CRPC therapy.

Acknowledgements

This study was supported by the Medical Scientific Research Foundation of Guangdong Province, China (Grant No. B2025003) and the Foshan Self-funded Science and Technology Innovation Project, China (Grant No. 2420001004198).

Disclosure of conflict of interest

None.

Address correspondence to: Wei Wei, Department of Urology, Foshan Hospital of Traditional Chinese Medicine Affiliated to Guangzhou University of Chinese Medicine, No. 6 Qinren Road, Chancheng District, Foshan 528000, Guangdong, China. E-mail: cn2weiwei@163.com; Ming Chen, Department of Urology, The First Affiliated Hospital of Guangzhou University of Chinese Medicine, Courtyard No. 16 Airport Road, Baiyun District, Guangzhou 510405, Guangdong, China. E-mail: chenming0953@163.com

References

[1] Bray F, Laversanne M, Sung H, Ferlay J, Siegel RL, Soerjomataram I and Jemal A. Global cancer statistics 2022: GLOBOCAN estimates of incidence and mortality worldwide for 36 cancers in 185 countries. CA Cancer J Clin 2024; 74: 229-263.

[2] Zhang Y, Ming A, Wang J, Chen W and Fang Z. PROTACs targeting androgen receptor signaling: potential therapeutic agents for castration-resistant prostate cancer. Pharmacol Res 2024; 205: 107234.

[3] Dai C, Dehm SM and Sharifi N. Targeting the androgen signaling axis in prostate cancer. J Clin Oncol 2023; 41: 4267-4278.

[4] Tilki D, van den Bergh RCN, Briers E, Van den Broeck T, Brunckhorst O, Darraugh J, Eberli D, De Meerleer G, De Santis M, Farolfi A, Gandaglia G, Gillessen S, Grivas N, Henry AM, Lardas M, J L H van Leenders G, Liew M, Linares Espinos E, Oldenburg J, van Oort IM, Oprea-Lager DE, Ploussard G, Roberts MJ, Rouvière O, Schoots IG, Schouten N, Smith EJ, Stranne J, Wiegel T, Willemse PM and Cornford P. EAU-EANM-ESTRO-ESUR-ISUP-SIOG guidelines on prostate cancer. Part II-2024 update: treatment of relapsing and metastatic prostate cancer. Eur Urol 2024; 86: 164-182.

[5] Armstrong AJ, Lin P, Tombal B, Saad F, Higano CS, Joshua AM, Parli T, Rosbrook B, van Os S and Beer TM. Five-year survival prediction and safety outcomes with enzalutamide in men with chemotherapy-naïve metastatic castration-resistant prostate cancer from the PREVAIL trial. Eur Urol 2020; 78: 347-357.

[6] Shore ND, Laliberté F, Ionescu-Ittu R, Yang L, Mahendran M, Lejeune D, Yu LH, Burgents J, Duh MS and Ghate SR. Real-world treatment patterns and overall survival of patients with metastatic castration-resistant prostate cancer in the US prior to PARP inhibitors. Adv Ther 2021; 38: 4520-4540.

[7] Qin D, Han S, Liu M, Guo T, Hu Z, Zhou Y and Luo F. Polysaccharides from Phellinus linteus: a systematic review of their extractions, purifications, structures and functions. Int J Biol Macromol 2023; 230: 123163.

[8] Yu K, Tan Z and Xin Y. Systematic evaluation of the anti-tumor effect of Phellinus linteus polysaccharide in thyroid carcinoma in vitro. Mol Biol Rep 2022; 49: 2785-2793.

[9] Syukriya AJ, Bankeeree W, Prasongsuk S and Yanatatsaneejit P. In vitro antioxidant and anticancer activities of Smilax corbularia extract combined with Phellinus linteus extract against breast cancer cell lines. Biomed Rep 2023; 19: 63.

[10] Yu T, Ganapathy S, Shen L, Peng B, Kim SH, Makriyannis A and Chen C. A lethal synergy induced by phellinus linteus and camptothecin11 in colon cancer cells. Oncotarget 2018; 9: 6308-6319.

[11] Hussain M, Fizazi K, Shore ND, Heidegger I, Smith MR, Tombal B and Saad F. Metastatic hormone-sensitive prostate cancer and combination treatment outcomes: a review. JAMA Oncol 2024; 10: 807-820.
[12] Azad AA, Kostos L, Agarwal N, Attard G, Davis ID, Dorff T, Gillessen S, Parker C, Smith MR, Sweeney CJ, Tombal B and Fizazi K. Combination therapies in locally advanced and metastatic hormone-sensitive prostate cancer. Eur Urol 2025; 87: 455-467.
[13] Tsuji T, Du W, Nishioka T, Chen L, Yamamoto D and Chen CY. Phellinus linteus extract sensitizes advanced prostate cancer cells to apoptosis in athymic nude mice. PLoS One 2010; 5: e9885.
[14] Zhu T, Guo J, Collins L, Kelly J, Xiao ZJ, Kim SH and Chen CY. Phellinus linteus activates different pathways to induce apoptosis in prostate cancer cells. Br J Cancer 2007; 96: 583-590.
[15] Masood M, Rasul A, Sarfraz I, Jabeen F, Liu S, Liu X, Wei W, Li J and Li X. Hispolon induces apoptosis against prostate DU145 cancer cells via modulation of mitochondrial and STAT3 pathways. Pak J Pharm Sci 2019; 32: 2237-2243.
[16] Kou F, Mei Y, Wang W, Wei X, Xiao H and Wu X. Phellinus linteus polysaccharides: a review on their preparation, structure-activity relationships, and drug delivery systems. Int J Biol Macromol 2024; 258: 128702.
[17] Wu Y, Liu H, Li Z, Huang D, Nong L, Ning Z, Hu Z, Xu C and Yan JK. Purification of polysaccharides from Phellinus linteus by using an aqueous two-phase system and evaluation of the physicochemical and antioxidant properties of polysaccharides in vitro. Prep Biochem Biotechnol 2022; 52: 89-98.
[18] Han J, Wu T, Jin J, Li Z, Cheng W, Dai X, Yang K, Zhang H, Zhang Z, Zhang H, Fan R, Zheng S, Liu H, Li Y, Zhao H, Yao C, Lin T, Zhu C and Liu H. Exosome-like nanovesicles derived from Phellinus linteus inhibit Mical2 expression through cross-kingdom regulation and inhibit ultraviolet-induced skin aging. J Nanobiotechnology 2022; 20: 455.
[19] Peng Y, Wang Y, Zhou C, Mei W and Zeng C. PI3K/Akt/mTOR pathway and its role in cancer therapeutics: are we making headway? Front Oncol 2022; 12: 819128.
[20] Li Q, Li Z, Luo T and Shi H. Targeting the PI3K/AKT/mTOR and RAF/MEK/ERK pathways for cancer therapy. Mol Biomed 2022; 3: 47.
[21] Lyu P, Li F, Deng R, Wei Q, Lin B, Cheng L, Zhao B and Lu Z. Lnc-PIK3R1, transcriptionally suppressed by YY1, inhibits hepatocellular carcinoma progression via the Lnc-PIK3R1/miR-1286/GSK3β axis. Biochim Biophys Acta Mol Basis Dis 2024; 1870: 167233.
[22] Martling A, Hed Myrberg I, Nilbert M, Grönberg H, Granath F, Eklund M, Öresland T, Iversen LH, Haapamäki C, Janson M, Westberg K, Segelman J, Ersson U, Prytz M, Angenete E, Bergström R, Mayrhofer M, Glimelius B and Lindberg J. Low-dose aspirin for PI3K-altered localized colorectal cancer. N Engl J Med 2025; 393: 1051-1064.
[23] Liu Y, Wang D, Li Z, Li X, Jin M, Jia N, Cui X, Hu G, Tang T and Yu Q. Pan-cancer analysis on the role of PIK3R1 and PIK3R2 in human tumors. Sci Rep 2022; 12: 5924.
[24] Cobleigh MA, Layng KV, Mauer E, Mahon B, Hockenberry AJ and Abukhdeir AM. Comparative genomic analysis of PIK3R1-mutated and wild-type breast cancers. Breast Cancer Res Treat 2024; 204: 407-414.
[25] Wang K, Hu Y, Xu L, Zhao S, Song C, Sun S, Li X and Li M. A novel mutant PIK3R1 (EY451delinsD) breast cancer patient resistant to HER2-targeted therapy treated with everolimus: a case report. Mol Biol Rep 2022; 49: 6155-6160.
[26] Cai J, Chen Z, Zhang Y, Wang J, Zhang Z, Wu J, Mao J and Zuo X. CircRHBDD1 augments metabolic rewiring and restricts immunotherapy efficacy via m(6)A modification in hepatocellular carcinoma. Mol Ther Oncolytics 2022; 24: 755-771.
[27] Gupta I and Gaykalova DA. Unveiling the role of PIK3R1 in cancer: a comprehensive review of regulatory signaling and therapeutic implications. Semin Cancer Biol 2024; 106-107: 58-86.
[28] Pungsrinont T, Kallenbach J and Baniahmad A. Role of PI3K-AKT-mTOR pathway as a pro-survival signaling and resistance-mediating mechanism to therapy of prostate cancer. Int J Mol Sci 2021; 22: 11088.
[29] Turnham DJ, Bullock N, Dass MS, Staffurth JN and Pearson HB. The PTEN conundrum: how to target PTEN-deficient prostate cancer. Cells 2020; 9: 2342.
[30] Tortorella E, Giantulli S, Sciarra A and Silvestri I. AR and PI3K/AKT in prostate cancer: a tale of two interconnected pathways. Int J Mol Sci 2023; 24: 2046.
[31] Brina D, Ponzoni A, Troiani M, Calì B, Pasquini E, Attanasio G, Mosole S, Mirenda M, D'Ambrosio M, Colucci M, Guccini I, Revandkar A, Alajati A, Tebaldi T, Donzel D, Lauria F, Parhizgari N, Valdata A, Maddalena M, Calcinotto A, Bolis M, Rinaldi A, Barry S, Rüschoff JH, Sabbadin M, Sumanasuriya S, Crespo M, Sharp A, Yuan W, Grinu M, Boyle A, Miller C, Trotman L, Delaleu N, Fassan M, Moch H, Viero G, de Bono J and Alimonti A. The Akt/mTOR and MNK/eIF4E pathways rewire the prostate cancer translatome to secrete HGF, SPP1 and

BGN and recruit suppressive myeloid cells. Nat Cancer 2023; 4: 1102-1121.
[32] Raith F, O'Donovan DH, Lemos C, Politz O and Haendler B. Addressing the reciprocal crosstalk between the AR and the PI3K/AKT/mTOR signaling pathways for prostate cancer treatment. Int J Mol Sci 2023; 24: 2289.
[33] Sen A, Khan S, Rossetti S, Broege A, MacNeil I, DeLaForest A, Molden J, Davis L, Iversrud C, Seibel M, Kopher R, Schulz S and Laing L. Assessments of prostate cancer cell functions highlight differences between a pan-PI3K/mTOR inhibitor, gedatolisib, and single-node inhibitors of the PI3K/AKT/mTOR pathway. Mol Oncol 2025; 19: 225-247.
[34] Qian L, Zhu Y, Deng C, Liang Z, Chen J, Chen Y, Wang X, Liu Y, Tian Y and Yang Y. Peroxisome proliferator-activated receptor gamma coactivator-1 (PGC-1) family in physiological and pathophysiological process and diseases. Signal Transduct Target Ther 2024; 9: 50.
[35] LeBleu VS, O'Connell JT, Gonzalez Herrera KN, Wikman H, Pantel K, Haigis MC, de Carvalho FM, Damascena A, Domingos Chinen LT, Rocha RM, Asara JM and Kalluri R. PGC-1α mediates mitochondrial biogenesis and oxidative phosphorylation in cancer cells to promote metastasis. Nat Cell Biol 2014; 16: 992-1003, 1-15.
[36] Hoxhaj G and Manning BD. The PI3K-AKT network at the interface of oncogenic signalling and cancer metabolism. Nat Rev Cancer 2020; 20: 74-88.